6.2 MODELING INACTIVATION OF B. ANTHRACIS BY ULTRAVIOLET RADIATION, PART I: DATA AND ANALYSIS

Stephanie L. Seely[1] and John M. Shuford
ENSCO Inc., Melbourne, FL

1. INTRODUCTION

This presentation is one of three to summarize preliminary experimental work performed jointly by ENSCO Inc. and Battelle Memorial Institute to determine a method for modeling the rate of inactivation of spores of *Bacillus anthracis*, the causative agent of anthrax, under arbitrary environmental conditions using observed weather data. For part I, we present a summary of our methods and a short synopsis of the analysis of the laboratory data.

For 40 years the bioterrorism domestic preparedness and the battlefield defense communities have had minimal information about the decay of *B. anthracis* as a Biological Weapons agent under natural sunlight. The often cited rate of decay of this microorganism in spore form for clear sky conditions under bright sunlight is 2% loss per minute (Beebe, *et al.*, 1962; US Army, 1992). This rate is often assumed to hold for solar noon, regardless of location or time of year, and is reduced by a sinusoidal function of sun angle for all other times of day. The rate is typically reduced by an *ad hoc* factor to account for cloudy conditions or poor visibility. Until recently, no research has supported any other quantitative estimate of the sensitivity of *B. anthracis* in spore form to sunlight.

2. EXPERIMENT DESCRIPTION

A bioaerosol containment chamber in a BL-3 laboratory at Battelle Memorial Institute's Medical Research and Evaluation Facility was used to expose *B. anthracis* spores (Ames strain) in aerosol form to UV radiation. A nebulization source was used to generate a nearly monodisperse aerosol of the spores into a holding chamber, from which the aerosol was delivered to two 18 inch by 1 inch diameter stainless steel sampling tubes. One tube was exposed to a simulated solar light source, the other was maintained dark as a control. Following the exposure period, gelatin filters were used to collect the sample from each tube.

Collimated light from a 1000 Watt Xenon light source (Oriel #6269) was directed at an angle of 45^{o} onto a dichroic UV reflecting filter (Oriel #66236) which reflects wavelengths between approximately 280 and 400 nm. The light then passed through one of various long-pass cutoff filters, then through a VIS-IR bandpass blocking filter (Oriel #81015) to irradiate the experimental test chamber through a quartz window in the bottom of the exposure tube.

A fiber optic probe connected to a spectroradiometer (Ocean Optics Instruments, S2000-UV-VIS, SAD500) above a second quartz window at the top of the exposure tube sampled spectral irradiance at the beginning of each exposure. The spectroradiometer was calibrated once daily using a 30 Watt deuterium third-tier NIST traceable irradiance standard (Oriel #63345, 68840).

The optical long-pass filters varied the spectral distribution of the UV energy by permitting transmission of longer wavelength light above a specified cut-off wavelength. All but one of the filters were colored glass-type, with nominal cut-off wavelengths at 285, 299, and 324 nm (Oriel #59423, 59425, and 59458). The remaining filter (atmospheric attenuation filter) was used to attenuate wavelengths below 300 nm (Oriel #81017).

Relative humidity was maintained constant (20% +/- 5%), as was the aerosol concentration in the chamber (1.0E+3 +/- 1.0E+1) and the temperature (27^{o}). The variable conditions were light spectrum (selected by long-pass filter), light intensity (controlled by an analog voltage setting on the lamp (200, 400, 700, and 1000 Watts), and residence time (10 to 60 minutes). The upper limit of 60 minutes was necessary to minimize the effects of settling on the sampled concentrations.

3. DATA

The experimental design incorporated four power settings of the UV lamp, and five optical filters. Different combinations of power setting and filter produced variations in the spectral distribution of the UV irradiance. Different length exposures produced a range of fluence levels. Each experimental run yielded a survival fraction in the interval [0,1] calculated as the ratio N/N_o where N was the number of colony forming units (CFU) observed in live culture of the exposed group of organisms, and N_o was the CFU count for the control group (Table 1 through Table 3). Each survival fraction was paired with a measured UV irradiance spectrum. Spectral irradiance was recorded at 0.16 nm intervals within the range 280 to 450 nm.

Table 1: Experimental runs using the cg299 filter.

Filter, Power (W), Time (min)	Surviving Fraction	Total UV Irradiance mW/(m^{2}nm)	Peak UV Irradiance mW/(m^{2}nm)	Effective Irradiance[a] mW/(m^{2}nm) at 280 nm	d/h[b]
299-200-10	0.95	871.3	16.0	0.33	0.31
299-200-10	0.96	817.0	14.4	0.39	0.27
299-200-10	1.00	496.0	9.0	0.20	0.40
299-200-10	1.10	978.9	16.5	3.10	0.10
299-200-10	1.10	855.6	15.4	1.36	0.20
299-200-20	0.41	967.6	17.5	0.61	0.19

1. Corresponding author address: 445 Pineda Ct., Melbourne, FL, 32940. email: seely.stephanie@ensco.com

Table 1: Experimental runs using the cg299 filter.

Filter, Power (W), Time (min)	Surviving Fraction	Total UV Irradiance mW/(m^{2}nm)	Peak UV Irradiance mW/(m^{2}nm)	Effective Irradiance[a] mW/(m^{2}nm) at 280 nm	d/h[b]
299-200-20	0.58	496.0	9.0	0.20	0.40
299-200-20	0.74	1037.4	19.1	0.98	0.20
299-200-20	0.74	885.9	15.5	5.89	0.11
299-200-20	0.81	1415.8	26.9	0.39	0.28
299-200-20	0.93	1162.0	21.2	0.64	0.20
299-200-30	0.25	1030.7	18.2	0.45	0.31
299-200-30	0.25	548.4	10.0	0.20	0.41
299-200-30	0.33	836.6	14.8	0.37	0.28
299-200-30	0.37	1398.7	25.1	1.41	0.13
299-200-30	0.37	928.7	18.7	0.26	0.23
299-200-30	0.42	932.4	16.0	1.81	0.17
299-200-30	0.58	763.2	14.2	0.19	0.45
299-200-30	0.63	1056.6	18.6	4.88	0.15
299-200-35	0.15	1055.4	17.8	4.16	0.16
299-200-35	0.46	979.4	15.6	10.44	0.16
299-200-40	0.21	903.2	14.8	6.61	0.18
299-200-45	0.19	839.3	15.4	0.29	0.36
299-200-45	0.39	963.4	18.0	0.35	0.25
299-400-5	0.64	2323.2	40.0	10.95	0.04
299-400-5	0.88	2205.1	38.2	4.58	0.06
299-400-5	0.93	3760.7	65.8	7.50	0.06
299-400-5	0.98	2557.1	44.4	7.22	0.06
299-400-5	1.00	2646.6	47.1	3.45	0.10
299-400-5	1.02	2734.7	46.9	4.92	0.09
299-400-10	0.34	3270.5	57.4	6.26	0.06
299-400-10	0.63	2419.4	41.2	8.17	0.05
299-400-10	0.64	1811.9	31.5	2.43	0.10
299-400-10	0.70	2744.2	47.2	4.18	0.10
299-400-10	0.75	2289.3	40.4	6.87	0.06
299-400-15	0.13	3208.3	56.8	7.99	0.04
299-400-15	0.14	3587.8	61.0	15.86	0.03
299-400-15	0.19	2998.9	52.3	6.02	0.07
299-400-15	0.24	2561.0	44.7	4.46	0.07
299-400-15	0.26	2010.6	36.4	1.68	0.13
299-400-15	0.30	1200.9	20.6	2.14	0.17
299-700-5	0.61	5714.6	98.7	10.11	0.04
299-700-5	0.69	4889.7	81.9	11.62	0.04
299-700-5	0.74	4214.0	70.3	11.43	0.04
299-700-5	0.87	3605.3	64.7	5.54	0.06
299-700-8	0.35	5097.8	88.4	13.45	0.03
299-700-8	0.36	5115.6	88.9	9.08	0.04
299-700-8	0.44	4198.8	70.8	14.94	0.03
299-700-10	0.07	5698.8	92.8	15.20	0.04
299-700-10	0.11	5086.5	86.9	31.83	0.03
299-700-10	0.33	4265.5	72.8	8.78	0.06
299-700-15	0.06	4226.5	70.5	16.43	0.03
299-700-15	0.09	4181.5	71.7	7.80	0.07

a.Effective irradiance was calculated using the Munakata *et al.* (1996) action spectrum normalized by its value at 280 nm.
b. To be discussed in "Modeling and Analysis"

Table 2: Experimental runs using the cg324 filter.

Filter, Power, Time	Surviving Fraction	Total UV Irradiance mW/(m^{2}nm)	Peak UV Irradiance mW/(m^{2}nm)	Effective Irradiance mW/(m^{2}nm) at 280 nm	d/h
324-700-60	1.00	3362.7	68.4	0.49	0.04
324-1000-60	1.00	6454.6	132	0.37	0.02

Table 3: Experimental runs using the AA filter.

Filter, Power, Time	Surviving Fraction	Total UV Irradiance mW/(m^{2}nm)	Peak UV Irradiance mW/(m^{2}nm)	Effective Irradiance mW/(m^{2}nm) at 280 nm	d/h
AA-400-60	0.30	1875.1	32.8	0.65	0.12
AA-400-60	0.37	2078.1	37.3	0.67	0.12
AA-400-60	0.42	1521.9	28.6	0.28	0.24
AA-400-60	0.52	1979.2	34.5	1.33	0.06
AA-400-60	0.76	1790.3	31.2	0.64	0.11
AA-700-45	0.94	1588.0	28.4	0.44	0.12
AA-700-60	0.10	2550.8	45.6	0.80	0.08
AA-700-60	0.13	5096.8	90.0	2.00	0.04
AA-700-60	0.23	1546.6	27.4	0.46	0.13
AA-700-60	0.25	2207.9	39.7	0.64	0.08
AA-700-60	0.31	5098.2	91.6	1.61	0.04
AA-700-60	0.33	4626.5	80.4	1.89	0.05
AA-700-60	0.47	4222.8	74.1	1.66	0.05
AA-700-60	0.55	4264.4	73.9	1.76	0.04
AA-1000-15	0.95	3435.2	62.5	1.04	0.05
AA-1000-30	0.58	1752.8	31.9	0.47	0.09
AA-1000-30	0.74	2530.7	44.7	0.75	0.08
AA-1000-30	0.91	8696.1	153	3.22	0.04
AA-1000-45	0.13	3650.0	66.6	0.93	0.11
AA-1000-45	0.48	2426.5	42.8	0.72	0.09

4. MODELING AND ANALYSIS

Background. Our objective is to obtain a statistical model with which we can predict the rate of loss of viability caused by a given, arbitrarily shaped UV irradiance spectrum. This presents a significant challenge, since the spectral distribution (by wavelength) of UV light output by a Xenon lamp in the laboratory is very different from the spectral distribution of energy in the solar spectrum. In fact, no one filter can adequately represent or mimic sunlight at the earth's surface. This is because the spectral distribution of solar radiation changes with the height of the sun in the sky. It also changes with variations in ozone column concentration, aerosol optical depth, reflectivity of the earth's surface, clouds, geography, and numerous other environmental factors. In other words, it is not adequate to model the response of the organism to a single spectral distribution, regardless of whether the spectrum is generated by a lamp or the sun.

The solution to this problem is a mathematical construct known as an action spectrum. This is a biological weighting function that describes the relative effectiveness of radiation in producing a specific biological effect as a function of wavelength. An action spectrum will be used to help interpret these exposure data, and after coupling with a radiative transfer model, will allow the transport model to predict loss of assayable material for any given, arbitrarily shaped solar spectrum.

In this section, we will show the exposure data do demonstrate somewhat of a coherent structure, and that from them we may determine a method for predicting the rate of loss of assayable material for any solar radiation environment.

Treatment of Irradiance Spectra. It is well known that the effectiveness of radiation in the UVB region (280 to

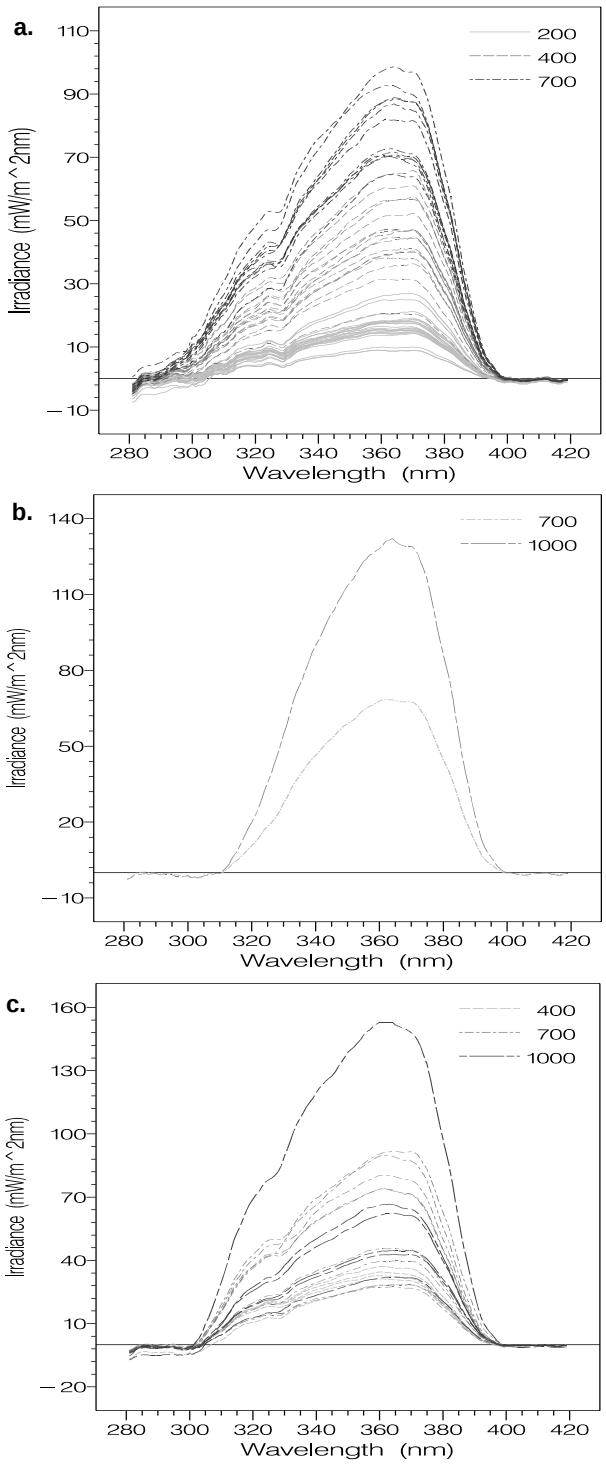

Figure 1. UV spectral irradiance using the a) cg299, b) cg324, and c) AA optical filter plotted by the lamp power setting.

315 nm) for destruction of biological material is much greater than that of radiation in the longer-wavelength UVA region. Therefore, destruction by UV exposure is more sensitively affected by small variations in UVB irradiance than by small variations in the UVA region. Dosimetric errors in the UVB region are therefore a potentially important source of random and/or systematic variability in our data.

One way in which the effects of dosimetric uncertainty are manifest in these data is the occurrence of negative irradiance values within most of the spectra shown in Figure 1. These negative values are understood to be artifacts from over-correction for detector dark signal. While occurrences of negative values at longer wavelengths (say, 400 nm and above) were of little concern because of the negligible effectiveness of ultraviolet radiation in that region, negative values at shorter wavelengths were troubling.

First Look at the Data. As a simplistic starting point, we examine fraction of viable material remaining (or survival of the spores) versus total UV fluence[1]. In Figure 2, the logarithm of fraction remaining is plotted versus total fluence; that is, the (non-negative) spectral irradiance integrated across wavelength multiplied by the exposure time. Due to the substantial dissimilarities among the irradiance spectra obtained with each of the optical filters with regard to the relative amounts of UVA and UVB present in the spectra, no clear overall trend is apparent.

Among the data obtained using the cg299 filter (circles) we can see a clear overall trend of decreasing suvival with increasing UV fluence. But due to significant differences among the irradiance spectra obtained with the AA filter (triangles), the AA data segregate into two clusters in this plot, each exhibiting an apparent association between spore inactivation and UV fluence.

Meanwhile, the two data points associated with the cg324 filter (dots) indicate a lack of decay at two large but distinctly different fluence values. The segregation of these data by optical filter and the distinct clusters in the AA filter results clearly attest to the inadequacy of total UV fluence—integrated without reference to the relative effectiveness of UV radiation at different wavelengths—as a predictor of loss of viability.

The Action Spectrum. We need a model that will account for the wavelength dependency on biological effect. An action spectrum serves as a weighting function: when an ultraviolet irradiance spectrum is multiplied by an action spectrum (appropriate to the biological effect in question) and integrated over the relevant wavelength interval, one obtains a measure of the effective irradiance to which an organism is exposed. That is, if $\varepsilon(\lambda)$ is an action spectrum, and $I(\lambda)$ is the measured irradiance[2] at wavelength λ, then the formula:

---

1. Since the negative irradiance values are not physically meaningful, we set irradiance to zero at all those wavelengths where a negative value had been recorded.
2. Here *I* represents irradiance and *F* is reserved for fluence, the time integral of irradiance. In general, *F* typically represents irradiance (flux).

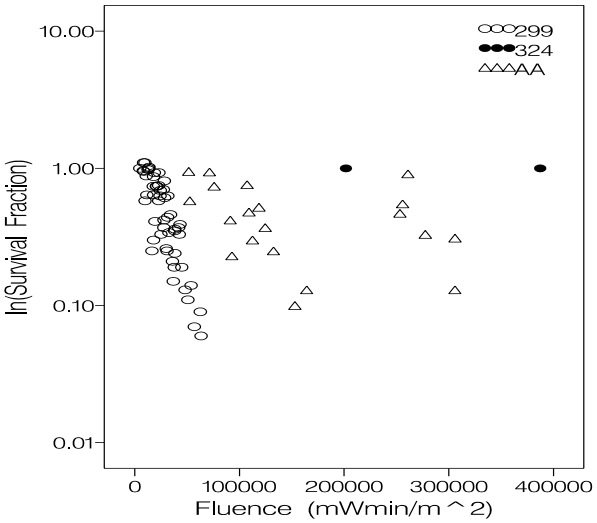

Figure 2. Ln(survival fraction) vs. UV fluence.

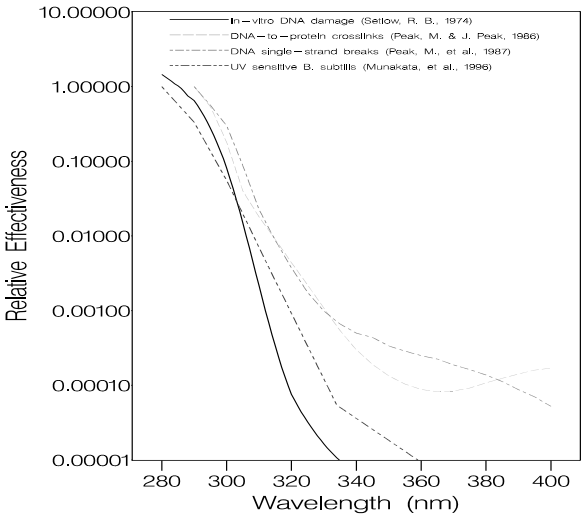

Figure 3. Several selected published action spectra.

$$I_{eff} = \sum_{\lambda} \varepsilon(\lambda) I(\lambda) \Delta\lambda \qquad (1)$$

expresses the biologically effective irradiance relative to the action spectrum $\varepsilon(\lambda)$.

In Figure 3, several published action spectra for various biological effects are shown. These action spectra describe relative effectiveness of UV light in damaging DNA *in vitro* (Setlow, 1974), producing single strand breaks in DNA (Peak *et al.*, 1987), producing DNA to protein crosslinks (Peak and Peak, 1986), and killing spores of a UV sensitive strain of *B. subtilis* (Munakata, *et al.*; 1996). (Note: the action spectra are normalized by their values at either 280 or 290 nm.) While there are differences among them both in their shape and in the methods by which they were estimated, a common feature is the log-linearity of scale -- that is, exponential declines in biological effectiveness with arithmetic increases in wavelength. The action spectrum obtained by Munakata, *et al.* (1996) is of particular interest because it describes the relative effectiveness of UV radiation for the inactivation of a UV-sensitive strain of *Bacillus subtilis*—an organism in the same genus as *Bacillus anthracis*.

Second Look at the Data. It would therefore be interesting -- even if only as a heuristic device -- to use these action spectra to weight the irradiance spectra shown in Figure 1 and then examine the relationship between loss of viability and biologically effective fluence. If the same physical mechanism that produced the wavelength dependence described by any of these action spectra is responsible for the loss of assayable material in this experiment, it is reasonable to conjecture that action spectrum would be appropriate for UV decay of *B. anthracis*. Figure 4 provides a plot of ln(survival) versus biologically effective fluence (as weighted by the Munakata *et al.* action spectrum normalized to unity at 280 nm). Contrasting Figure 4 with Figure 2, we see that the data associated with the four different optical filters now intermingle and present a more coherent relationship between ln(survival) and biologically effective fluence.

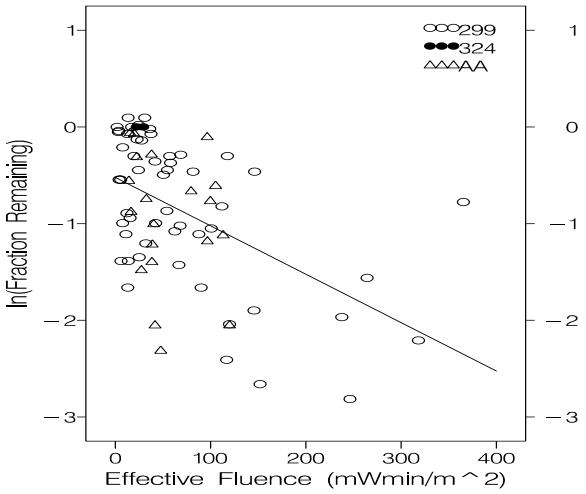

Figure 4. Ln(survival) vs. biologically effective fluence (as weighted by the Munakata, et al. action spectrum).

However, the least-squares fit through the data in Figure 4 has a particularly troubling feature: namely, the y-intercept (equal to -0.52) that is significantly different from zero. A y-intercept less than zero implies that on the basis of these data a significant amount of the inactivation would be expected even as the effective fluence approaches zero. This does not make sense physically, and it suggests one or more of the following problems:

1. that there are discordant data (aberrations either in dosimetry or assay results) distorting this fit,
2. that the action spectrum is inappropriate,

3. that the relationship between ln(survival) and effective fluence is misspecified as a first degree linear model, or
4. that uncontrolled nuisance factors have interfered with the experiment.

To investigate whether the first of these might be the case -- i.e. that measurement aberrations might be manifest in these data -- let us take a second look at the dosimetry data in the context of measurement uncertainty.

Theoretical Uncertainty in the Dosimetry. The spectroradiometer has the following specifications. The 1/4 meter, crossed Czerny-Turner design spectrometer accepts light energy transmitted through a single-strand optical fiber and disperses it via a fixed grating across a charge-coupled device type detector. The detector is a 2048-element linear array, where each element is 12.5 mm x 200 mm. The detector has a well depth of 160,000 photons, and a sensitivity of 86 photons/count (2.9×10^{-17} Joule/count). The grating has a density of 600 lines/mm, set to 200-850 nm (blazed at 300 nm), and the slit width is 25 μm with a height of 1000 mm. The detector has a single-piece, multi-bandpass coating to eliminate second-order effects from 200-850 nm. The instrument was calibrated for absolute irradiance once daily using a third-tier (NIST-traceable) 30 Watt deuterium standard.

Based on guidance provided in Kostkowski's *Reliable Spectroradiometry* (1997), specifications provided by the manufacturer, and educated guesses in the absence of documentation, we have estimated the uncertainty of the irradiance measurements (Table 4). The largest sources of uncertainty were due to noise in the measurement data, collection of collimated light using a fiber optic probe, assumed possible temperature shifts of 5^{o}C in the lab, transfer uncertainties of the 3rd tier deuterium standard and its drift due to frequent ignition, and possible polarization effects. (More will be said about noise shortly.) If the value of the uncertainty from each contributing source is squared, the squared values added together, and the square root taken of the sum, this value represents the total uncertainty. Twice that value represents the "expanded uncertainty" which is roughly equivalent to a 2-sigma estimate of total uncertainty. We estimate the 2 sigma uncertainty in these spectral irradiances is *at least* 20% at 300 nm.

Table 4: Estimated uncertainty (%) in spectral irradiance.

Source or Type of Uncertainty	250 nm	300 nm	350 nm
Size of Source Effects	n/a	n/a	n/a
Directional & Positional Effects[a]	5	5	5
Detector Instability[b]	9.5	5	~0
Drift in the Standard[c]	4.5	4.5	4.5
Uncertainty of the Standard[d]	4.4	4.35	4.3
Polarization Effects[e]	3	3	3
Noise in the measurement data[f]	>3.8	>2.5	~0
Instability of the Standard[g]	0.5	0.5	0.5
Instability of the Quantity being measured[h]	0.6	0.5	0.43
Spectral Scattering[i] ('Stray Light' Measurement by Ocean Optics)	0.1	0.1	0.1
Spectral Distortion[j]	0.1	0.1	0.1
Wavelength Instability[k]	0.1	0.1	0.1
Nonlinearity[l]			
Total Uncertainty (combined uncertainties in quadrature)	>13.4	>10.2	>8.6

a. interpreted here as error introduced by the appearance of modal structures in the field of collimated light as collected by the fiber optic--simply a guess--we hope it is worst case.

b. These values are estimated from a least-squares regression relationship using the correspondence between counts and irradiance for four cg285 spectra, an assumed maximum temperature shift of 5^{o}C and a subsequent shift of 10 counts at any wavelength.

c. This value represents the drift over time (30 / 100 hours x 5%) that has been multiplied by an *ad hoc* factor of 3 to account for the frequent ignition.

d. As listed on the calibration certificate.

e. An FEL standard is polarized approximately 3%, which is very likely a worst case value.

f. These values are estimated from a least-squares regression relationship using the correspondence between counts and irradiance for 4 cg285 spectra, and an assumed maximum error due to noise of 4 counts at any wavelength. However, the data seem to indicate a much higher value at wavelengths where the flux approached zero.

g. Here we are assuming a maximum of 0.5% uncertainty in the current (Kostkowski, 1997), and a 1:1 correspondence between uncertainty in the current measurement and irradiance uncertainty.

h. Here we are assuming the use of a high quality power supply with the UV solar simulator--which would allow us to assume the same uncertainties as an FEL Quartz-Tungsten-Halogen standard with a 0.05% uncertainty in the current measurement: 0.05% x 5(600/λ).

i. Probably a reasonable estimate given the unknown source spectrum was limited from 280 to 450 nm.

j. This is also a guess.
k. No wavelength calibrations were performed during the course of the experiment. We hope this is worst case.
l. We were unable to obtain any information on this source of uncertainty.

We would note for future experiments, many of these sources of uncertainty may be characterized more precisely, corrected for, and/or significantly reduced. The use of an FEL type absolute irradiance standard (1000 Watt Quartz-Tungsten-Halogen) would allow calibration of the spectroradiometer using a spectrum more similar to the unknown source. A diffuser must be added to the entrance optics, since a fiber optic alone is unsuitable for measurement of collimated light. Reliability of the data could be improved by performing regular wavelength calibrations, creating working irradiance standards and documenting intercomparisons of the three irradiance sources at regular intervals, recording multiple spectra and averaging them to optimize the signal to noise ratio, and reducing the lower limit of the wavelength interval to ensure measurement of the very small fluxes that may be present beyond a filter cutoff.

Since we have reason to suspect our estimated uncertainty due to noise at the lowest wavelengths is much too low, and since this wavelength region produces the largest biological effect, it is worthwhile to examine the data set again in this context. As a surrogate for the signal to noise ratio within a given irradiance spectrum, we calculated the ratio between the largest negative irradiance (d) and the peak irradiance (h) observed in a given spectrum. A tabulation of this fraction is listed in the rightmost columns of Table 1 through Table 3.

A reasonable strategy for screening the data would then be to set a threshold value for the ratio *d/h* and set aside from the analysis all experimental runs for which *d/h* exceeds the threshold. We have elected to set aside all observations for which *d/h* exceeds 10%--a total of 34 of the 75 observations in the data set. The majority of these are associated with the lowest lamp power setting, but because of the exponential increase of effectiveness with decreasing wavelength, radiometric errors in irradiance at these very short wavelengths contributed a large part of the total effective irradiance for these low-power spectra. And this uncertainty would be magnifed by multiplication by the longer exposure times associated with these irradiance spectra.

Third Look at the Data. An obvious question to answer at this point would be whether the data screening just applied eliminates the significantly negative intercept in the least-squares fit of ln(survival) versus effective fluence, where biological effectiveness is weighted according to the action spectrum of Munakata, *et al.*. The answer is yes. Using the 41 observations that passed our screening criterion, we now obtain the fit shown in Figure 5 and the regression estimates as found in Table 5.

Although it was derived from an experiment involving a close relative of our subject organism, our use thus far of the Munakata, *et al.* action spectrum to weight the irradiance spectra from this experiment has been heuristic. We have yet to address the question of whether an action spectrum for the UV inactivation of *B. anthracis* can be obtained from an analysis of our experimental data. To accomplish this, we have adapted an approach described by Rundel (1983) for estimating action spectra from polychromatic exposures. The approach can be characterized by the following:

Table 5: Summary of results obtained from first-order regression of ln(survival) on the predictor variable effective_fluence, where biological effectiveness is weighted according to the action spectrum of Munakata, *et al.* using screened data.

Model: ln(survival) ~ effective_fluence				
Coefficients	Value	Std. Error	t value	Pr(>|t|)
intercept	-0.143	0.147	-0.971	0.338
effective_fluence	-0.00937	0.00143	-6.54	0.00
Residual standard error: 0.588 on 39 degrees of freedom				
Multiple R-Squared: 0.523				
F-statistic: 42.7 on 1 and 39 degrees of freedom, p-value: 9.31e-8				

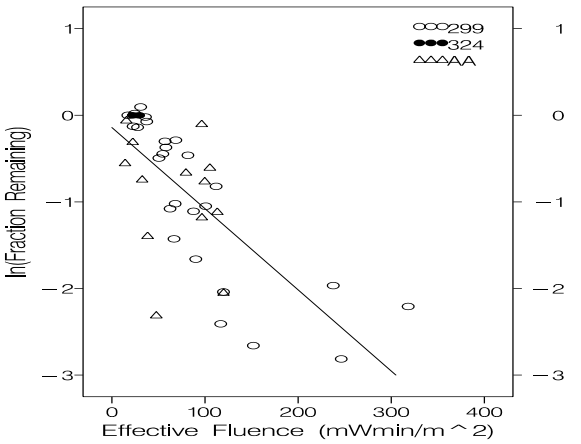

Figure 5. Relationship between ln(survival) and biologically effective UV fluence relative to the Munakata, *et al.* action spectrum with screened data.

1. Assume a parametric form for an action spectrum $\varepsilon(\lambda)=\varepsilon(\lambda|\theta)$ where θ is a vector of real parameters. For example, θ might be a vector of four real numbers describing a cubic function of λ:

$$\varepsilon(\lambda) = \theta_1\lambda^3 + \theta_2\lambda^2 + \theta_3\lambda + \theta_4 \quad (2)$$

2. Calculate biologically effective irradiance:

$$I_{eff}(\theta)_j = \sum_{\lambda} \varepsilon(\lambda|\theta) \cdot I_j(\lambda) \quad (3)$$

3. Next, calculate the biologically effective fluence

$$F_{eff}(\theta)_j = I_{eff}(\theta)_j T_j \quad (4)$$

where T_j is the exposure time (in minutes) for experimental run *j*.

4. Now search for $\hat{\theta}$ that maximizes the success in using $F_{eff}(\theta)_j$ as a predictor of the biological effect observed in experimental run *j*. Specifically, our approach was to find $\hat{\theta}$ that maximizes the coefficient of determination (R^2) for the simple linear regression model:

$$\log(Y_j) = \beta_0 + \beta_1 F_{eff}(\theta)_j + e_j \quad (5)$$

where Y_j is the fraction remaining (i.e., N/N_0) observed on experimental run *j*.

Following this approach, let us first assume the functional form:

$$\varepsilon(\lambda|\theta) = e^{-\theta(\lambda - 280)} \quad (6)$$

for $280 < \lambda < 400$ where θ is a scalar (note that this form normalizes the biological effectiveness to a value of 1.0 at 280 nm). For simplicity, we tried candidate values for θ from the set {0.00, 0.01, 0.02, 0.03,..., 0.99, 1.00}. The maximum value of R^2 was obtained with the value $\hat{\theta}$=0.17; that is with the action spectrum:

$$\varepsilon(\lambda|\theta) = e^{-0.17(\lambda - 280)} \quad (7)$$

After the irradiance spectra in the data set were weighted with the action spectrum given by Equation 7, the linear regression fit obtained for the model given by Equation 7 is summarized in Table 6.

Table 6: Summary of results obtained from first-order regression of ln(survival) on the predictor variable effective_fluence, where biological effectiveness is weighted according to the action spectrum $\varepsilon(\lambda|\theta) = e^{-0.17(\lambda - 280)}$.

Model: ln(survival) ~ effective_fluence				
Coefficients	Value	Std. Error	t value	Pr(>|t|)
intercept	-0.104	0.158	-0.658	0.515
effective_fluence	-0.0133	0.00213	-6.25	0.00
Residual standard error: 0.602 on 39 degrees of freedom				
Multiple R-Squared: 0.500				
F-statistic: 39.014 on 1 and 39 degrees of freedom, p-value: 2.36e-7				

A Relationship for the Transport Model. The observation that the estimated intercept in the first-order regression summarized in Table 6 was not significantly different from zero and that effective fluence is a ratio-scale quantity -- along with the physical argument that the absence of effective UV fluence should result in zero destruction of assayable material due to this mode of decay -- motivated us to respecify the statistical model without an intercept term; i.e. to regress through the origin. And since the Munakata *et al.* action spectrum produced a better fit, it was selected for use in calculating effective irradiance. A summary of such a regression analysis is presented in Table 7.

As a prerequisite to the use of this relationship within the transport model, it is important to ask whether the range of UV irradiance conditions normally encountered in the environment (near ground level) falls within

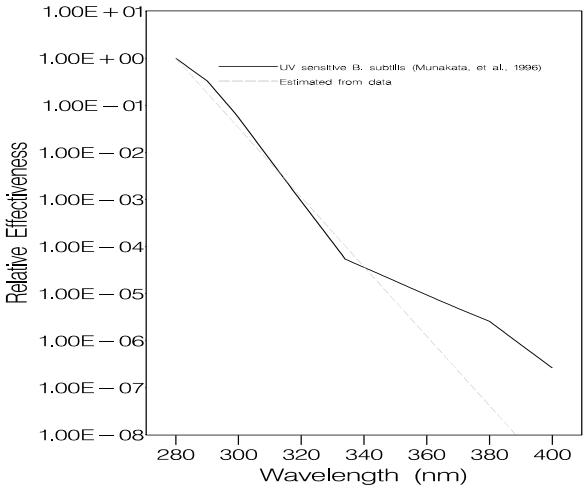

Figure 6. An estimated action spectrum for UV inactivation of *B. anthracis*.

Table 7: As in Table 6, summary of results obtained from first-order regression (without an intercept).

Model: ln(survival) ~ effective_fluence				
Coefficients	Value	Std. Error	t value	Pr(>|t|)
effective_fluence	-0.0105	0.0009	-11.679	0.00
Residual standard error: 0.588 on 40 degrees of freedom				
Multiple R-Squared: 0.773				
F-statistic: 136.4 on 1 and 40 degrees of freedom, p-value: 1.83e-14				

the range of effective irradiance values within our experimental data. For comparison, in Table 8 below, three representative environmental modeling scenarios are examined. The first of these corresponds to solar noon at 23.5° N latitude on the summer solstice -- a harsh UV environment thought to represent the extreme of likely modeling scenarios. This solar spectrum was generated using the software package FASTRT (Engelsen and Kylling, 1998), the others were observed solar spectra obtained with permission from van Weele, *et al.* (2000).

We observe that effective irradiance in the data set ranged between 0.37 to 31.8 mW/m^2 at 280 nm. Correspondingly, effective fluence ranged from 14.2 to 318.3 mWmin/m^2. The estimates of environmental effective irradiance as well as the effective fluence in a 10-minute period slightly exceed the range of values observed in the experiment. But the harshest scenario would be operationally relevant only in rare circumstances and for short time periods. In any case, is important to note that most of the lamp's effectiveness for inactivation is due to excessive amounts of UVB, and that the amount of UVA radiation output by the lamp is far less than that output by the sun. Nevertheless, the range of effective radiation in this data set does approximate the range that could be encountered in the outside environment.

Table 8: Illustration of uncertainty in individual predicted surviving fraction for three representative bioaerosol modeling scenarios.[a]

Scenario	Effective Irradiance	Effective Fluence[b]	Predicted ln(survival)	95% confidence interval
Summer Solstice	34.1	341	-3.58 +/- 1.34	0.01 to 0.11
Midlatitude, High Sun	9.15	91.5	-0.96 +/- 1.20	0.12 to 1.0
Midlatitude, Low Sun	0.184	1.84	-0.02 +/- 1.19	0.30 to 1.0

a. Uncertainties represent lower bounds on prediction error.
b. via Munakata *et al.* (1996)

5. SUMMARY

A set of experimental data including UV radiation dosimetry measured by a spectroradiometer and the resulting observed inactivation of *B. anthracis* spores was examined. A linear least-squares regression relationship was determined between ln(fraction remaining) and effective fluence. That relationship may be expressed as:

$$\frac{N}{N_0} = e^{-kUVt}, \quad (8)$$

where N/N_0 is the fraction of assayable material remaining, *UV* is total effective irradiance, *t* is time, *UVt* is effective fluence, and *-k* is the slope of the regression line (-0.0105). In order to apply this relationship to a particular environmental scenario, the term *UV* must be calculated using a radiative transfer model and the appropriate weather data. Then *kUV* becomes the new decay constant for an exponential relationship to predict ln(fraction remaining) after time *t* within that solar radiation environment.

Also, the inactivation action spectrum determined from this data set was similar to another AS published for a similar organism. When either AS was used to weight the dosimetry data, a log-linear relationship was apparent between survival of the organism and the effective UV dose. This relationship held regardless of the spectral distribution of the UV radiation. Because the Munakata, *et al.* action spectrum produced a better fit, it was selected for use.

This correspondence permitted the design of an algorithm to predict inactivation of the organism under arbitrary environmental conditions. Since the range of effective fluence in the experimental data was similar to the highest levels that might be experienced in the environment over a period of 10 minutes, the algorithm timestep should be limited to 10 minutes or less.

The results of this work in progress are promising, and plans are to repeat the experiment with several corrections to the radiometric measurement setup now that the feasiblity of the sample aerosolization method has been successfully tested.

6. REFERENCES

Beebe, J.M. *et al.* August 1962. Stability and Virulence Relationships of Airborne Bacillus Anthracis Spores under Stress of Light and Humidity, (Technical Memorandum No. 18). Aerobiology Division, U.S. Army Biological Laboratories, Frederick, Maryland.

Engelsen, O. and Kylling, A. (1998) "Fast radiation transfer modeling of downward UV doses, indices and irradiances at the Earth's surface", European Conference on Atmospheric UV Radiation, Helsinki, 28 June - 2 July 1998. http://zardoz.nilu.no/~olaeng/fastrt/fastrt.html

Headquarters, Dept. of the Army, 16 November 1992, Chemical and Biological Contamination Avoidance, Field Manual No. 3-3, Washington D.C..

Kostkowski, H. (1997) Reliable Spectrradiometry. Spectroradiometry Consulting, P.O. Box 2747, La Plata, MD, 20646-2747, 609 pp.

Munakata, N., Morohoshi, F., Hieda, K., Suzuki, K., Furusawa, Y., Shimura, H., and Ito, T. (1996) Experimental correspondence between spore dosimetery and specral photometry of solar ultraviolet radiation. Photochemistry and Photobiology, 63, 74-78.

Peak, J.J., and Peak J.G. (1986) DNA-to-protein crosslinks and backbone breaks caused by far- and near-ultraviolet, and visible radiations in mammalian cells. In Mechanisms of DNA Damage and Repair. Implications for Carcinogenesis and Risk Assessment, (Edited by M.G. Simic, L. Grossman and A.C. Upton), 193-202, Plenum Press, New York.

Peak, M.J., Peak, J.G., and Carnes, B.A. (1987) Introduction of direct and indirect single-strand breaks in human cell DNA by far-and near-ultraviolet radiations: Action spectrum and mechanisms. Photochemistry and Phtobiology, 45, 381-387.

Rundel, R.D. (1983) Action spectra and estimation of biologically effective UV radiation. Physiol Plant, 58, 360-366.

Setlow, R.B. (1974) The wavelengths in sunlight effective in producing cancer: a theoretical analysis. Proceedings of the National Academy of Sciences U.S.A., 71: 3363-3366.

van Weele, M., Martin, T.J., Blumthaler, M., Brogniez, C., den Outer, P.N., Engelsen, O., Lenoble, J., Mayer, B., Pfister, G., Ruggaber, A., Walravens, B., Weihs, P., Gardiner, G.G., Gillotay, D., Haferl, D., Kylling, A., Seckmeyer, G., and Wauben, W.M.F. (2000) From model intercomparison toward benchmark UV spectra for six real atmospheric cases. Journal of Geophysical Research (Atm), 105, 4915-4925.